Chinese Chemical Letters 35 (2024) 109384

Contents lists available at ScienceDirect

Chinese Chemical Letters

journal homepage: www.elsevier.com/locate/cclet

Inhaled multilevel size-tunable, charge-reversible and mucus-traversing composite microspheres as trojan horse: Enhancing lung deposition and tumor penetration

Lishan Xiong[a], Xinyuan Li[a], Xiaojie Lu[a], Zhendong Zhang[a], Yan Zhang[a], Wen Wu[b,*], Chenhui Wang[a,*]

[a] Chongqing Key Laboratory of Natural Product Synthesis and Drug Research, School of Pharmaceutical Sciences, Chongqing University, Chongqing 401331, China

[b] Chongqing Key Laboratory of High Active Traditional Chinese Drug Delivery System, Chongqing Engineering Research Center of Pharmaceutical Sciences, Chongqing Medical and Pharmaceutical College, Chongqing 404120, China

ARTICLE INFO

Article history:
Received 5 November 2023
Revised 5 December 2023
Accepted 6 December 2023
Available online 15 December 2023

Keywords:
Pulmonary delivery
Size-tunable nanoparticles
Charge-reversible nanoparticles
Mucus penetration
Lung cancer

ABSTRACT

Dry powder inhalation represents a promising approach for the treatment of lung cancer, offering several advantages such as enhanced targeting, improved bioavailability, and reduced toxicity. However, traditional dry powder formulations suffer from limitations, notably low pulmonary delivery efficiency and inadequate penetration into tumor tissues, thereby limiting their therapeutic efficacy. In response to these challenges, we have developed an innovative trojan horse strategy, harnessing an inhalable nanoparticle-in-microsphere system characterized by tunable size, reversible charge, and mucus-penetrating capabilities. The inhalable nanoparticle-in-microsphere system exhibit stable structural properties, excellent environmental responsiveness and high biocompatibility. More importantly, the therapeutic effect of MTX@PAMAM@HA@Gel (MPHG) was demonstrated *in vitro* and *in vivo*. This system offers improved pulmonary delivery efficiency, enhanced drug retention within tumor tissues, and effective penetration, thus representing a promising strategy in lung cancer treatment.

Pulmonary drug delivery systems have emerged as a promising approach for the treatment of lung diseases, offering advantages such as targeted delivery, improved bioavailability, and reduced systemic side effects [1–3]. Among various pulmonary drug delivery methods, dry powder inhalers (DPIs) are considered convenient and propellant-free, making them an attractive option for patients [4,5]. However, efficient drug delivery to the lungs and deep penetration into tumor tissues remain significant challenges [6–9].

Powders for DPIs need to be formulated with an aerodynamic diameter in the range of 1–5 μm which is considered as the most suitable particle size for pulmonary inhalation to reach and deposit in the deep lungs [10–14]. However, carriers with such particle sizes are susceptible to clearance by the immune system present in the lungs, posing a challenge for reaching pulmonary tumor tissues [15,16]. Nanoparticles are more likely to evade clearance mechanisms by the lung defense systems [17,18]. Notably, ultra-small nanoparticles (~50 nm) exhibit excellent tumor tissue penetration abilities [19–21]. However, they are easily exhaled after inspiration and cannot achieve deep lung deposition [17,22,23]. Thus, there is a contradiction in selecting carrier sizes that are both efficient for deep lung deposition and effective in penetrating tumor tissues.

Beyond the particle size of carriers, the surface charge is another crucial factor affects lung cancer therapy [24–27]. Negative charge facilitate the drug delivery system to traverse multiple respiratory pathways and reach deep into the lung tissues, while positive charge promotes its uptake by tumor cells [28,29]. Therefore, the differing requirements for charge at different sites pose a second challenge in achieving both deep lung delivery and tumor tissue uptake simultaneously.

Besides, achieving effective pulmonary drug delivery faces significant challenges posed by the body's innate defense mechanisms, primarily the thick mucus layer and mucociliary clearance [30–33]. When inhaled delivery systems come into contact with this mucus layer, they can become trapped due to various physicochemical interactions, including hydrophobic, electrostatic, and van der Waals forces [34] and eventually be swallowed or expelled

* Corresponding authors.
E-mail addresses: wuwen1988@cqu.edu.cn (W. Wu), wangchenhui@cqu.edu.cn (C. Wang).

https://doi.org/10.1016/j.cclet.2023.109384
1001-8417/

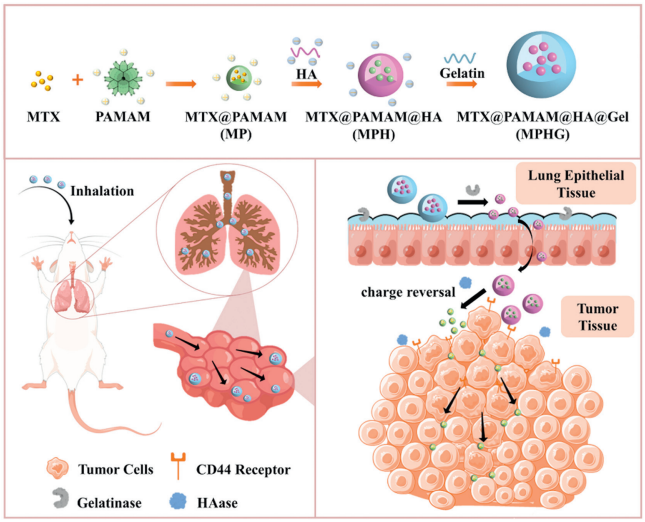

Fig. 1. Schematic illustration for multilevel size-tunable, charge-reversible and mucus-traversing inhaled composite microspheres for the treatment of lung cancer.

through coughing [35,36]. Considering the substantial impact of mucociliary clearance on the efficiency of intratracheal and pulmonary drug delivery, the development of delivery systems with mucus-penetrating capabilities is imperative for achieving successful pulmonary drug delivery [37–39].

Herein, we propose a novel approach utilizing inhaled multilevel size-tunable, charge-reversible and mucus-traversing composite microspheres as trojan horses, aiming to enhance drug delivery and improve lung cancer therapy (Fig. 1). The composite microspheres offer the potential to address the three key challenges of inadequate lung deposition, ineffective mucus penetration and limited tumor tissue penetration. Small particles loaded with the anticancer drug methotrexate (MTX), denoted as MTX@PAMAM (MP), were encapsulated within hyaluronic acid (HA) nanoparticles, forming a formulation referred to as MTX@PAMAM@HA (MPH) [40]. Subsequently, inhalable nanoparticle-carrier composite microspheres MTX@PAMAM@HA@Gel (MPHG) encapsulating MPH nanoparticles were prepared using gelatin (Gel) as the carrier matrix. Upon the delivery of MPHG to the lungs, the gelatin shells undergo rapid dissolution due to enzymatic action and temperature, resulting in the release of MPH. This marks the first stage of particle size alteration, effectively addressing the challenge of pulmonary delivery inefficiency. Furthermore, as the released MPH is transported to the tumor sites, it undergoes rapid degradation facilitated by hyaluronidase (HAase), an enzyme overexpressed in tumor tissues. This enzymatic degradation leads to the liberation of the enclosed MP spheres, consequently enhancing the drug's penetration into tumor tissues. Rigorous evaluations demonstrated that these composite microspheres not only enhance pulmonary drug delivery efficiency but also significantly improve drug penetration within tumor tissues. Consequently, the composite microspheres MPHG present a promising vehicle for the pulmonary delivery of chemotherapeutic agents for treatment of lung cancer.

In this study, we have selected the fourth-generation poly(amidoamine) (PAMAM) as the ideal carrier for delivering the therapeutic drug MTX. Its small particle size facilitates improved penetration of tumor tissue, enabling deep delivery of the drug into the affected tissue. As illustrated in Table S1 (Supporting information) and Fig. 2A, the particle size of MP was measured at 5.38 ± 0.35 nm and demonstrated exceptional dispersibility. The drug loading of MP was 42.61% ± 0.83%. In order to prepare nanoparticles (MPH) with good properties, the influence of formulation and process variables on the characteristics of nanoparticles was assessed (Tables S2–S5 in Supporting information). The final molecular weight of hyaluronic acid selected was 600 kDa, the organic solvent was acetone, the experimental stirring speed was 600 rpm, and the feeding ratio of HA and MP was 5:2. And the average particle size of MPH was determined to be 266.31 ± 1.92 nm (Table S1, Fig. 2B, and Fig. S1 in Supporting information). The polydispersity index (PDI) indicated a satisfactory particle size distribution. The encapsulation efficiency was 47.15% ± 6.96%, and drug loading was determined to be 7.05% ± 0.66%. Moreover, the zeta potential measurements revealed that MP, blank HA nanoparticles, and MPH possessed zeta potentials of $+13.79 \pm 1.17$, -25.11 ± 0.62, and -20.96 ± 0.72 mV, respectively. These results suggested the successful loading of MP into HA nanoparticles, facilitated by the abundant positive charge associated with the primary amine group on the PAMAM surface.

The study meticulously explored the influence of various formulation and process variables on the characteristics of microspheres (MPHG). After thorough experimentation, as shown in Fig. S2–S5 (Supporting information), an optimal preparation process was established. This process involves using gelatin with a strength of 300 bloom, Span 80 as the emulsifier, and a mixing speed of 800 rpm. The proportion of gelatin to MPH was carefully adjusted to a ratio of 5:1. The resulting microspheres demonstrated exceptional dispersion and homogeneity, as evidenced in Table S1, Fig. 2C, and Fig. S6 (Supporting information). The average particle size of these microspheres was measured to be 3773.33 ± 683.91 nm. Notably, this size range aligns perfectly with the required specifications (1–5 μm) for pulmonary dry powder inhalers, a critical application in drug delivery systems as referenced in study [41]. Furthermore, the encapsulation efficiency of the MPHG microspheres was impressively high at 85.87% ± 7.73%. Additionally, the drug loading capacity was determined to be 1.06% ± 0.05%.

To validate the successful construction of the drug delivery system, the distribution of fluorescence generated by the microspheres was observed using laser confocal microscopy. Rhodamine B-labeled gelatin and FITC@PAMAM@HA (FPH) prepared using the same procedure by replacing MTX with fluorescein isothiocyanate (FITC) were incorporated into the composite microspheres to enhance visibility for confocal microscopy. The red fluorescence emitted by rhodamine B-labeled gelatin exhibited a spherical morphology and the green fluorescence from FPH was evenly distributed throughout the red carrier (Fig. 2D and Fig. S7 in Supporting information). These results collectively confirm the successful construction of the composite microspheres. In the infrared characteristic spectrogram (Fig. S8 in Supporting information), the spectra of MPHG exhibited none of the characteristic peaks of MPH but rather those of gelatin microspheres, further indicating the effective encapsulation of MPH into gelatin microspheres.

To investigate the particle size change ability of MPH, we conducted an incubation experiment with HAase. MPH exhibited excellent stability in phosphate buffered saline (PBS) (Fig. 2E). However, after a 2-h incubation with HAase, the particle size of the nanoparticles significantly decreased to less than 10 nm (Fig. 2F). This observation clearly demonstrates that MPH can effectively undergo particle size reduction in response to HAase stimulation. Similarly, to assess the particle size change ability of MPHG, we incubated MPHG with collagenase type IV (Cls IV). It was observed that the larger micron-sized particles gradually decreased, while the smaller micron-sized particles increased and shifted towards smaller particle sizes (Fig. 2G). Moreover, as the incubation time increased, the nanoscale particles further shifted towards smaller sizes (Fig. 2H). *In vitro* degradation maps of microspheres taken by inverted microscopy (Fig. 2I) validated these findings. Initially, the microspheres exhibited stable morphology and uniform size. And most of the microspheres had undergone degradation at 4–8 h. The degradation experiments confirm that gelatin microspheres

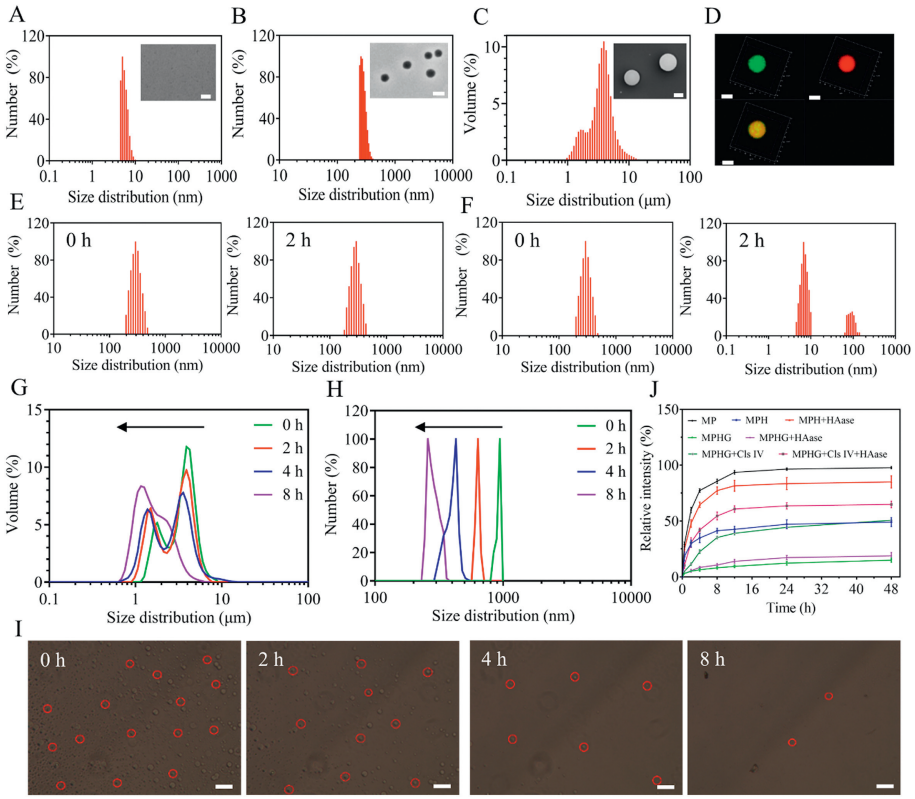

Fig. 2. Characterization of MPHG. (A) Size and morphology of MP. Scale bar: 50 nm. (B) Size and morphology of MPH. Scale bar: 500 nm. (C) Size and morphology of MPHG microspheres. Scale bar: 2 μm. (D) The fluorescence distribution inside the microspheres by laser confocal microscopy. Scale bar: 5 μm. (E) Degradation particle size of MPH in PBS without HAase. (F) Degradation particle size of MPH in PBS with HAase. (G) Degradation particle size of MPHG at four time points of 0, 2, 4, and 8 h were determined at the micron level. (H) Degradation particle size of MPHG at four time points of 0, 2, 4, and 8 h were determined at the nanometer level. (I) Degradation morphology of MPHG at four time points of 0, 2, 4, and 8 h. Scale bar: 50 μm. (J) Release curves of MP, MPH and MPHG under different conditions.

can rapidly degrade under the dual stimulation conditions of collagenase and physiological temperature.

The *in vitro* release of MTX from both MPH and MPHG systems in buffered solutions with different enzymes was evaluated, and we found that the presence of enzymes greatly increases the rate of drug release (Fig. 2J). Also in the absence of enzymes, no abrupt drug release was observed, indicating that the carrier exhibited good stability.

Next, the cellular uptake of FITC@PAMAM (FP), FPH, and FITC@PAMAM@HA@Gel (FPHG) by A549 cells was investigated using laser confocal microscopy and flow cytometry. As depicted in Fig. 3A, A549 cells incubated with FP exhibited stronger fluorescence compared to those treated with FPH. This difference can be attributed to the negatively charged zeta potential and larger particle size of FPH compared to the positively charged FP. In the FPH + HAase group, the green fluorescence intensity was significantly increased compared to the FPH group. Similarly, the FPHG + Cls IV + HAase group exhibited enhanced absorption compared to the FPHG group. Flow cytometry analysis (Figs. 3B and C) corroborated the observations made with laser confocal microscopy, confirming that in the presence of enzymes, the particles can efficiently degrade and release the encapsulated FP nanoparticles, thereby enhancing the uptake of the drug by tumor cells.

The penetration capability of FP, FPH, and FPHG was evaluated in A549 tumor spheroids. As shown in Fig. 3D, both the FP group and the FPH + HAase group exhibited stronger green fluorescence compared to the FPH group. Additionally, the green fluorescence in the FP group and FPH + HAase group was uniformly distributed throughout the entire tumor spheroid, while in the FPH group, most of the green fluorescence was concentrated in the peripheral part of the spheroid. The FPHG group, due to its larger particle size, was unable to penetrate deeply and remained attached to the surface of the tumor spheroid. However, the FPHG + Cls IV + HAase group exhibited a tendency for inward penetration. The slower fluorescence penetration observed in this group may be attributed to the sustained release of the microspheres. These results demonstrate that the FPH and FPHG designed and constructed in this study have the ability to penetrate deep into tumor tissues in the presence of enzymes, which is crucial for enhancing the efficacy of chemotherapeutic drugs.

Then, the transport ability of particles across the mucus layer of the lungs was evaluated by Calu-3 cell monolayer model in the transwell plate (Fig. 3E). After a 6-hour incubation period, it was observed that the green fluorescence associated with FP particles remained predominantly at the surface of the mucus layer. This phenomenon may be attributed to the positive charge of FP, which hindered its penetration into the mucus layer. In the case of FPHG, a significant portion of the particles was retained within the upper layer of mucus, while a smaller fraction exhibited a tendency to permeate deeper into the mucus. This behavior could be attributed to the interplay between the larger particle size and mass. Conversely, FPH particles demonstrated superior mucus penetration compared to the other two groups. Consequently, it was inferred that following the deposition of microsphere particles deep within the lungs on the alveolar surface, FPHG could be effectively retained within the pulmonary environment due to both the weight of the microspheres and the adhesive properties of gelatin to mucus. Subsequently, FPH particles could be gradually released in response to enzymatic activity and changes in temperature, facilitating their uptake by lung tissues.

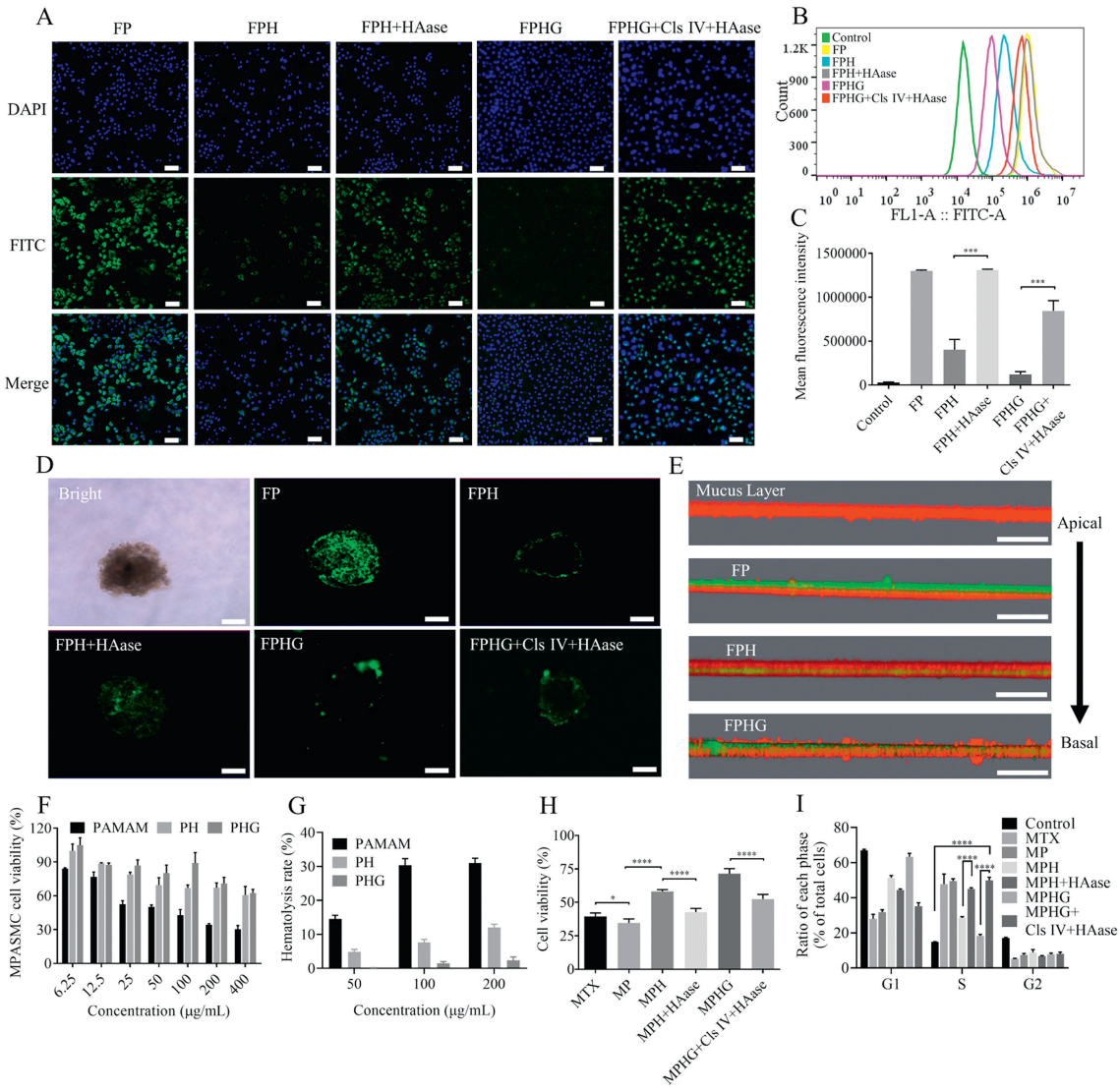

Fig. 3. Therapeutic efficient and safety evaluation of MPHG *in vitro*. (A) Laser confocal microscopy images of A549 cells uptake of FP, FPH, FPH+ HAase, FPHG and FPHG + Cls IV + HAase. Scale bar: 100 μm. (B) Flow cytometry analysis of cellular uptake of FP, FPH, FPH+ HAase, FPHG and FPHG + Cls IV + HAase in A549 cells. (C) Quantitative analysis of the flow cytometry data ($n = 3$). (D) Penetrating capability of FP, FPH, FPH + HAase, FPHG and FPHG + Cls IV + HAase on A549 tumor spheroids. Scale bar: 150 μm. (E) The transport ability of particles across the mucus layer was evaluated by CLSM in the transwell plate. The red and green fluorescence represent the mucus and particles, respectively. Scale bar: 50 μm. (F) The cytotoxicity profiles of blank carriers (PAMAM, PH, PHG) in MPASMC at different concentrations measured by MTT assays ($n = 6$). (G) Hemolysis percentage of PAMAM, PH and PHG at different concentrations ($n = 3$). (H) MTT assay for the cytotoxicity of MTX, MP, MPH, MPH + HAase, MPHG and MPHG + Cls IV + HAase to A549 cells ($n = 6$). (I) Quantitative analysis of the cell cycle analysis graphs in control, MTX, MP, MPH, MPH + HAase, MPHG and MPHG + Cls IV + HAase ($n = 3$). Data are presented as mean ± standard deviation (SD). $^{*}P < 0.05$, $^{***}P < 0.001$, $^{****}P < 0.0001$.

The cytotoxicity of PAMAM was investigated using the MTT assay to assess whether the complex microspheres could effectively reduce its toxicity (Fig. 3F, Figs. S9–S11 in Supporting information). The PAMAM exhibits significant cytotoxicity towards normal cells (MPASMC, RAW 264.7, 293T and L02). In contrast, the cell survival rate is significantly improved in the PAMAM@HA (PH) and PAMAM@HA@Gel (PHG) groups, with minimal cytotoxicity observed at lower concentrations and high cell survival rates maintained even at higher concentrations. Furthermore, blood compatibility is imperative for carriers [42], so a hemolysis assay was employed using mouse red blood cells to evaluate the blood compatibility of PAMAM, PH, PHG (Fig. 3G and Fig. S12 in Supporting information). PAMAM dendrimers has a toxicity which induced 31.03% hemolysis at 200 μg/mL. And pH exhibited a smaller hemolysis rate, demonstrating that HA encapsulated can significantly reduce the hemolytic toxicity of PAMAM. The percentage of hemolysis observed after sufficient contact between the PHG and blood was very low which is less than 2% at 200 μg/mL. These results indicate that the encapsulation of PAMAM by gelatin and hyaluronic acid can effectively inhibit its toxicity, demonstrating the safety of the PH and PHG systems.

The inhibitory effects of MP, MPH, and MPHG on A549 cells' proliferation were investigated (Fig. 3H). The cell viability of the MP group was lower compared to the MTX group, indicating that PAMAM loading enhances the uptake of the drug and that PAMAM itself possesses some toxicity. Additionally, the presence of enzymes effectively enhanced the anti-tumor activity of MPH and MPHG, further demonstrating the ability of the drug delivery system to modulate particle size. Cell cycle arrest induced by the microspheres was analyzed using flow cytometry (Fig. 3I and Fig. S13 in Supporting information). We found that administration of MP resulted in S-phase arrest in A549 cells, consistent with the effects of MTX compared to the untreated control cells. And the treatment groups with specific enzymes exhibited similar cell cycle inhibition

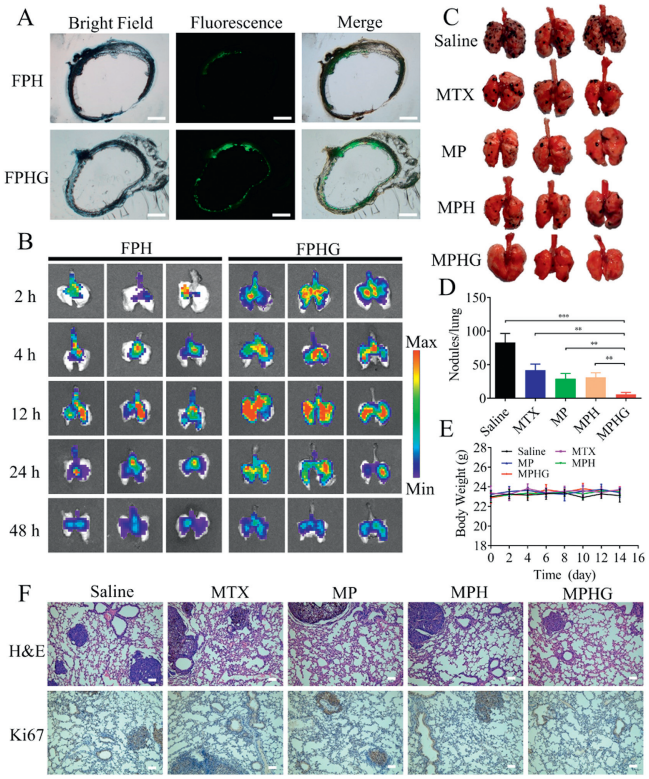

Fig. 4. Therapeutic efficient evaluation of MPHG *in vivo*. (A) Frozen section of tracheas from mice following inhalation administration of FPH and FPHG observed by inverted fluorescence microscope. Scale bar: 250 μm. (B) *In vivo* fluorescent images of lungs of mice after administration of FPH and FPHG. (C) Appearances of the lungs after treatment. (D) Quantification of lung metastasis nodules. (E) Body weight changes of the tumor-bearing mice were measured during 2 weeks post treatment. (F) H&E and Ki67 staining of the lung tissue sections. Scale bar: 75 μm. Data are expressed as the mean ± SD ($n = 5$). $^{**}P < 0.01$, $^{***}P < 0.001$.

effects to the MTX group, indicating that the enzymes effectively degraded the drug particles and released MP. These findings highlight the fact that the encapsulation of multilayer materials did not compromise the efficacy of methotrexate *in vivo*.

Pulmonary administration was performed in BALB/c mice to investigate the distribution of FPH and FPHG in the airways. In this study, all animal experiments were performed according to the guidelines approved by the Laboratory Animal Welfare and Ethics Committee of Chongqing University (No. CQU-IACUC-RE-202308-008). The fluorescence intensity of FPHG was significantly higher than that of FPH (Fig. 4A), which suggests that FPHG exhibits good retention in the respiratory tract. Besides, the lung deposition and retention of FITC-loaded nanoparticles and microspheres were analyzed in BALB/c mice. The distribution of microspheres in the lungs was visualized using an imaging system (Fig. 4B). The fluorescence intensity in the lungs was notably stronger in the FPHG microspheres group compared to the FPH nanoparticles group. These findings confirm that gelatin encapsulation enhances the lung deposition properties of FPH nanoparticles and facilitates deeper delivery of FPH nanoparticles into the lungs. Additionally, the microspheres effectively accumulated in the lungs within 48 h, and the fluorescent signals in the lungs gradually decreased over time, indicating the excellent lung targeting and retention capabilities of the FPHG microspheres.

A lung cancer-bearing BALB/c mice model was established *via* lateral tail vein injection with B16F10 cells to investigate the anti-lung cancer effects of MPHG microspheres. Compared to the negative control group, the lung tumors in each treatment group exhibited varying degrees of decrease, with the MPHG treatment group demonstrating the most significant efficacy (Figs. 4C and D). Throughout the treatment period, the mice's body weight remained relatively stable (Fig. 4E), indicating the safety of the administered drug in the organism. In the observation of hematoxylin-and-eosin staining and Ki67 staining of lungs, we found that the untreated group displayed numerous melanomas and pigmentations (Fig. 4F). In contrast, the lungs of the treated groups exhibited evident reductions in melanoma size and number, with the presence of normal pores, particularly in the MPHG group. Additionally, the MPHG-treated group demonstrated fewer Ki67-positive cells, further supporting the superior efficacy of MPHG. Normal mice were administered the drug and their major organs and blood were collected for toxicity analysis. Histological analysis of the heart, spleen, and kidney images revealed no apparent inflammation, damage, or edema in any of the five groups (Fig. S14 in Supporting information). Hematological analysis results showed that although there were slight variations in some indicators at 1 day and 7 days, the values of alanine aminotransferase (ALT), aspartate transaminase (AST) and blood urea nitrogen (BUN) in the mice remained within the normal range (Figs. S15–S17 in Supporting information). These findings indicate that the administered drugs are generally safe and do not induce damage to the liver and kidney [43].

In summary, the MPHG system represents an innovative approach to address the challenges associated with drug delivery to the lungs and deep penetration into tumor tissues using dry powder inhalation. The incorporation of multiple layers in the system, including gelatin, hyaluronic acid, PAMAM dendrimers, and MTX, allows for precise control over particle size variation, charge reverse and mucus penetration which are critical for optimal drug delivery. Our design is further validated through relevant experiments. Thus, the composite microspheres are promising for treating various diseases of the lung *via* pulmonary administration.

Declaration of competing interest

The authors declare that they have no known competing financial interests or personal relationships that could have appeared to influence the work reported in this paper.

Acknowledgments

This research was supported by the National Natural Science Foundation of China (No. 52273123), the Natural Science Foundation of Chongqing, China (No. CSTB2022NSCQ-MSX0474), and the Talent-introduction Program of Chongqing Medical and Pharmaceutical College (No. YGZRC2023103).

Supplementary materials

Supplementary material associated with this article can be found, in the online version, at doi:10.1016/j.cclet.2023.109384.

References

[1] M. Lau, P.M. Young, D. Traini, Drug Dev. Ind. Pharm. 43 (2017) 1229–1238.
[2] Y. Wang, L.H. Zhu, A.Z. Chen, et al., Materials 9 (2016) 368.
[3] A. Goel, S. Baboota, J.K. Sahni, J. Ali, Int. J. Pharm. Investig. 3 (2013) 8–14.
[4] T. Fischer, I. Winter, R. Drumm, M. Schneider, Pharmaceutics 13 (2021) 844.
[5] P. Muralidharan, M. Malapit, E. Mallory, D. Hayes Jr., H.M. Mansour, Nanomed. Nanotechnol. Biol. Med. 11 (2015) 1189–1199.
[6] H.J. Lee, J.H. Kang, H.G. Lee, et al., Drug Des. Devel. Ther. 10 (2016) 4017–4030.
[7] W. Wang, Q.T. Zhou, S.P. Sun, et al., AAPS J. 18 (2016) 372–384.
[8] Y. Xu, H.M. Liu, L. Song, J. Nanobiotechnol. 18 (2020) 145.
[9] N. Bungert, M. Kobler, R. Scherliess, Pharmaceutics 14 (2022) 951.
[10] J. Li, Y. Wang, C. Xu, et al., Acta Biomater. 134 (2021) 546–558.
[11] T. Parumasivam, R.Y.K. Chang, S. Abdelghany, et al., Adv. Drug Deliv. 102 (2016) 83–101.
[12] F. Depreter, G. Pilcer, K. Amighi, Int. J. Pharm. 447 (2013) 251–280.

[13] M.Y. Yang, J.G.Y. Chan, H.K. Chan, J. Control. Release 193 (2014) 228–240.
[14] N. Chishti, S. Jagwani, D. Dhamecha, S. Jalalpure, M.H. Dehghan, Medicina 55 (2019) 294.
[15] K. Knap, K. Kwiecien, K. Reczynska-Kolman, E. Pamula, Regen. Biomater. 10 (2023) rbac099.
[16] R. Scherliess, S. Bock, N. Bungert, A. Neustock, L. Valentin, Eur. J. Pharm. Sci. 172 (2022) 106158.
[17] A. Umerska, N.A. Mugheirbi, A. Kasprzak, P. Saulnier, L. Tajber, Powder Technol. 364 (2020) 507–521.
[18] Y. He, C. Liu, R. Han, et al., Chin. Chem. Lett. 34 (2023) 107484.
[19] D. Luo, X.N. Wang, C. Burda, J.P. Basilion, Cancers 13 (2021) 1825.
[20] Y. Niu, J. Zhu, Y. Li, et al., J. Control. Release 277 (2018) 35–47.
[21] H. Cabral, Y. Matsumoto, K. Mizuno, et al., Nat. Nanotechnol. 6 (2011) 815–823.
[22] M. Passi, S. Shahid, S. Chockalingam, I.K. Sundar, G. Packirisamy, Int. J. Nanomed. 15 (2020) 3803–3826.
[23] J. Du, I.M. El-Sherbiny, H.D. Smyth, AAPS PharmSciTech 15 (2014) 1535–1544.
[24] J. Zhao, L. Qin, R. Song, et al., Eur. J. Pharm. Biopharm. 172 (2022) 101–111.
[25] A.S. Alshetaili, Saudi. J. Biol. Sci. 28 (2021) 5065–5073.
[26] T.C. Hsiao, C.L. Han, T.T. Yang, et al., Environ. Sci. Pollut. Res. 30 (2023) 18985–18997.
[27] Q. Liu, J. Guan, L. Qin, X. Zhang, S. Mao, Drug Discov. Today 25 (2020) 150–159.
[28] X.M. Mao, S. Wu, P. Calero-Perez, et al., Cancers 14 (2022) 410.
[29] J.L. Xia, H.Y. Tian, J. Chen, et al., Polymers 8 (2016) 141.
[30] W.H. Wang, Z.W. Huang, Y. Huang, et al., Adv. Drug Deliv. Rev. 185 (2022) 114309.
[31] J.T. Huckaby, S.K. Lai, Adv. Drug Deliv. Rev. 124 (2018) 125–139.
[32] D.B. Hill, B. Button, M. Rubinstein, R.C. Boucher, Physiol. Rev. 102 (2022) 1757–1836.
[33] S.S. Hu, Z.X. Yang, S. Wang, et al., Chem. Eng. J. 428 (2022) 132107.
[34] X. Murgia, P. Pawelzyk, U.F. Schaefer, et al., Biomacromolecules 17 (2016) 1536–1542.
[35] A.J. Hibbitts, J.M. Ramsey, J. Barlow, R. MacLoughlin, S.A. Cryan, Nanomaterials 10 (2020) 1248.
[36] A.E. de Azevedo-Pereira, J.A. Saka, K.A. de Oliveira-Braga, et al., Clinics 68 (2013) 702–709.
[37] Y. Tang, L.F. Zhang, R. Sun, et al., Asian J. Pharm. 18 (2023) 100833.
[38] H.M. Ren, L. Han, L.J. Zhang, et al., Nano Today 44 (2022) 101489.
[39] Y. Liu, J.Y. Shen, J.P. Shi, et al., Chem. Eng. J. 427 (2022) 131742.
[40] M. Huo, W. Li, A. Sen Chaudhuri, et al., Carbohydr. Polym. 171 (2017) 173–182.
[41] Q. Wang, L. Ge, L. Wang, et al., Chin. Chem. Lett. 32 (2021) 1071–1076.
[42] R. Zhang, T. Nie, L. Wang, et al., Biomater. Sci. 11 (2023) 4254–4264.
[43] H. Chen, Z. Liu, B. Wei, et al., Bioact. Mater. 6 (2021) 655–665.